

# Raman and inelastic neutron scattering spectra of $(\text{NH}_4)_2\text{SO}_3$ , an intermediate for solar hydrogen production

Raúl E. Orozco-Mena, Stewart F. Parker,  
Eduardo F. Herrera-Peraza, David Chávez-Flores,  
Hernando Romero-Paredes and  
Víctor H. Ramos-Sánchez

## Published version information

**Citation:** RE Orozco-Mena et al. "Raman and inelastic neutron scattering spectra of  $(\text{NH}_4)_2\text{SO}_3$ , an intermediate for solar hydrogen production." International Journal of Hydrogen Energy, vol. 42, no. 51 (2017): 30216-30222.

**DOI:** [10.1016/j.ijhydene.2017.10.094](https://doi.org/10.1016/j.ijhydene.2017.10.094)

©2017. This manuscript version is made available under the [CC-BY-NC-ND](https://creativecommons.org/licenses/by-nc-nd/4.0/) 4.0 Licence.

This version is made available in accordance with publisher policies. Please cite only the published version using the reference above. This is the citation assigned by the publisher at the time of issuing the AAM. Please check the publisher's website for any updates.

**Raman and inelastic neutron scattering spectra of (NH<sub>4</sub>)<sub>2</sub>SO<sub>3</sub>, an intermediate for solar hydrogen production**

**Raúl E. Orozco-Mena,<sup>a</sup> Stewart F. Parker,<sup>b</sup> Eduardo F. Herrera-Peraza,<sup>a</sup>  
David Chávez-Flores,<sup>c</sup> Hernando Romero-Paredes<sup>d</sup> and  
Víctor H. Ramos-Sánchez<sup>\*c</sup>**

*<sup>a</sup>Medio Ambiente y Energía, Centro de Investigación en Materiales Avanzados, S.C., Miguel de Cervantes #120, Complejo Industrial Chihuahua, Chihuahua, Chih., México. C.P. 31136.*

*<sup>b</sup>ISIS Pulsed Neutron and Muon Facility, Science and Technology Facilities Council, Rutherford Appleton Laboratory, Harwell, Didcot, Oxfordshire, OX11 0QX, UK*

*<sup>c</sup>Cuerpo Académico de Química Aplicada y Educativa, Facultad de Ciencias Químicas, Universidad Autónoma de Chihuahua, Nuevo Campus Universitario, Circuito Universitario, Chihuahua, Chih., México. C.P. 31125.*

*<sup>d</sup>Área de Ingeniería en Recursos Energéticos, Universidad Autónoma Metropolitana-Iztapalapa, Av. San Rafael Atlixco 186, Col. Vicentina, México, D.F., México. C.P. 09340,*

<sup>\*</sup>Tel: +52 (614)2366000, mail: vramos@uach.mx

Keywords: Solar Thermochemical Cycle, Photolytic oxidation, Ammonium sulfite, Raman scattering, Inelastic neutron scattering.

## **Abstract**

The sulfur-ammonia (S-NH<sub>3</sub>) cycle uses the entire solar radiation spectrum to split water. It uses the UV radiation to promote the photolytic oxidation of ammonium sulfite to produce hydrogen and ammonium sulfate. Here, Raman and inelastic neutron scattering spectra of (NH<sub>4</sub>)<sub>2</sub>SO<sub>3</sub>·H<sub>2</sub>O at 20 K are discussed, supported by density functional theory (DFT) calculations. The feasibility of photolytic oxidation of this monohydrate to produce hydrogen at room temperature was also demonstrated.

## 1. Introduction

Hydrogen is an energy vector capable of replacing fossil fuels and providing energy for transportation, industry and households. Such a sustainable model scenario, known as the hydrogen economy, demands finding new methods to produce hydrogen on a large scale, while keeping the use of fossil fuels to a minimum and replacing steam reforming, which is the most widely used process to obtain hydrogen nowadays. Among the viable options are the Thermo Chemical Water Splitting Cycles (TCWSCs). In particular, the sulfur family cycles have been shortlisted as the most promising routes to obtain hydrogen on a large scale. European research projects such as HYTHEC and HYCYCLES have focused on studying the Sulfur-Iodine cycle and the Hybrid Sulfur cycle, respectively [1,2]. An innovative photothermochemical cycle within the same family has been developed: the sulfur-ammonia (S-NH<sub>3</sub>) cycle [3,4]. This cycle exploits the entire solar radiation spectrum to split water. It uses the UV radiation to promote the photolytic oxidation of ammonium sulfite to produce hydrogen and ammonium sulfate, an energy carrier and a potential fertilizer respectively, according to Reaction 1.



This step produces high purity hydrogen at room temperature, and it is usually carried out in solution [3-8]. Recent efforts to enhance exploitation of the solar spectrum, within the cycle, relied on the use of photocatalysts, such as CdS and CdSeZnS, which exhibit known toxicity issues [9]. However, even in presence of photocatalysts, quantum efficiency of the photolytic reaction is inherently limited due to water's UV absorption. Moreover, it is also logical to think that the overall efficiency of the S-NH<sub>3</sub> cycle is adversely affected by excess water in

subsequent operation units that involve water handling. Indeed, the theoretical particle model for the oxygen sub-cycle, lately reported, made evident the implication of managing water in a solar aerosol based reactor [10]. Therefore, an obvious choice would be to explore the reaction in the solid state by directly irradiating ammonium sulfite monohydrate  $((\text{NH}_4)_2\text{SO}_3 \cdot \text{H}_2\text{O})$ .

At this point, it is worthy to mention that sulfur-containing compounds are not only relevant in different areas, such as environmental science [11,12], food science [13], health [14], and material science [15]; but in particular, sulfate solutions  $((\text{NH}_4)_2\text{SO}_4$ , among these) are also of interest in hydrogen production through electrolytic hydrogen evolution reaction [16,17]. Several studies have been conducted on their molecular structures, using vibrational spectroscopy. Since the Raman cross section of sulfur is particularly favourable, sulfites and sulfates have been investigated in solution, glassy state and solid state, often accompanied by infrared spectroscopy [18-25]. Raman spectroscopy has been also used to study other sulfur family cycle, the S-I cycle, to gain further insights into molecular dynamics of the solutions involved and chemical species occurring within [26-28]. A complementary technique, inelastic neutron scattering (INS) spectroscopy, exhibits a remarkable hydrogen cross section that allows to study either hydrogen bonding, hydrogenated species, adsorbed molecular hydrogen, and even proton conduction [29,30]. It is remarkable the extensive literature available on ammonium vibrational modes, as a counterion in different inorganic salts, obtained by INS [31-38].

Here we aim to demonstrate the feasibility of photolytic oxidation of  $(\text{NH}_4)_2\text{SO}_3 \cdot \text{H}_2\text{O}$  in the solid state to produce hydrogen using a UV laser source. We also report a comprehensive study of the vibrational modes of  $(\text{NH}_4)_2\text{SO}_3 \cdot \text{H}_2\text{O}$ , especially those associated with the

hydrogen bonding network, and to present the Raman and INS spectra of  $(\text{NH}_4)_2\text{SO}_4$  and  $\text{Na}_2\text{SO}_3$ , which have not been previously reported. The unique features to choose such techniques were the capability to promote a photochemical process, by irradiating the sample with a 244 nm UV laser within a Raman microscope; and in the case of simultaneous INS and Raman spectroscopy at 785 nm, very low temperature and very low photon energy, which enables the analysis of sulfites without alteration.

## **2. Materials and Methods**

### **2.1 Reagents**

Bulk powders of  $(\text{NH}_4)_2\text{SO}_3 \cdot \text{H}_2\text{O}$ ,  $(\text{NH}_4)_2\text{SO}_4$  and  $\text{Na}_2\text{SO}_3$  were packed into sample holders, which consist in a two flat-plate aluminium cell sealed with indium wire and a sapphire window at the top, as described elsewhere [39]. All reagents were high purity, 92% or better from Alfa Aesar, and were used without further purification. The aluminium cells were used for the simultaneous recording of the Raman and INS spectra at 20 K.

### **2.2 Vibrational Spectroscopy**

High resolution INS spectra ( $\sim 1.25\% \Delta E$ ) were recorded at 20 K with the TOSCA spectrometer at ISIS (Didcot, UK). Simultaneously, Raman spectra were recorded with a customized Renishaw InVia system with 785 nm excitation [39] with improved resolution of  $\sim 3 \text{ cm}^{-1}$  and Raman shift threshold of  $40 \text{ cm}^{-1}$ . Raman spectra were also recorded at room temperature for  $(\text{NH}_4)_2\text{SO}_3 \cdot \text{H}_2\text{O}$  using a Renishaw InVia Raman microscope with 244 nm excitation, this instrument has a resolution of  $8 \text{ cm}^{-1}$  and a Raman shift threshold of  $400 \text{ cm}^{-1}$ .

## 2.2 Computational Details

Density functional theory (DFT) calculations were carried out with the plane-wave pseudopotential method as implemented in CASTEP [40]. Initial structures of  $(\text{NH}_4)_2\text{SO}_3 \cdot \text{H}_2\text{O}$ ,  $(\text{NH}_4)_2\text{SO}_4$  and  $\text{Na}_2\text{SO}_3$  were based on the available crystallographic data [41-43]. Note that the lattice parameters were constrained to the experimental values, unless specified otherwise, during the molecular geometry optimisation. The generalized gradient approximation (GGA) Perdew–Burke–Ernzerhof (PBE) functional was used in conjunction with optimized norm-conserving pseudopotentials. The plane wave cutoff was 830 eV in all cases. The k-point sampling was done with Monkhorst-Pack grids of  $6 \times 6 \times 4$  (36 k-points),  $6 \times 4 \times 6$  (18 k-points) and  $6 \times 6 \times 6$  (42 k-points) for  $(\text{NH}_4)_2\text{SO}_3 \cdot \text{H}_2\text{O}$ ,  $(\text{NH}_4)_2\text{SO}_4$  and  $\text{Na}_2\text{SO}_3$  respectively. In all cases the residual forces were  $|0.009| \text{ eV } \text{\AA}^{-1}$ . After geometry optimization, the vibrational spectra were calculated at the  $\Gamma$ -point in the harmonic approximation using density-functional perturbation theory [44]. This procedure generates the vibrational eigenvalues and eigenvectors, which allows visualization of the modes within the Jmol 3D software [45] and is also the information needed to calculate the INS spectrum using the program ACLIMAX [46]. We emphasize that none of the calculated frequencies were scaled.

## 3. Results and Discussion

### 3.1 Photolytic Oxidation of $(\text{NH}_4)_2\text{SO}_3 \cdot \text{H}_2\text{O}$

**Figure 1** shows the evolution of the photolytic oxidation carried out within a Raman microscope using a 25 mW 244 nm UV laser focussed onto a crystal of  $(\text{NH}_4)_2\text{SO}_3 \cdot \text{H}_2\text{O}$ . As the reaction occurred, it was evidenced by the appearance of a band at *ca.*  $1086 \text{ cm}^{-1}$  related to the  $\text{SO}_4^{2-}$  ion ( $\nu_3$ ) and a weakening of the band *ca.*  $1692 \text{ cm}^{-1}$  corresponding to the

scissoring mode of water within the monohydrate; a broad and weak band is observable at *ca.*  $1437\text{ cm}^{-1}$  presumably due to the symmetric N-H bending mode of the ammonium ion [20,24]. Based on this observation, it is possible to infer the production of hydrogen, which led us to consider the potential application of using moderately concentrated solar radiation to promote this photochemical process. Further knowledge of the lattice dynamics was then required, but avoiding chemical degradation of the monohydrate.

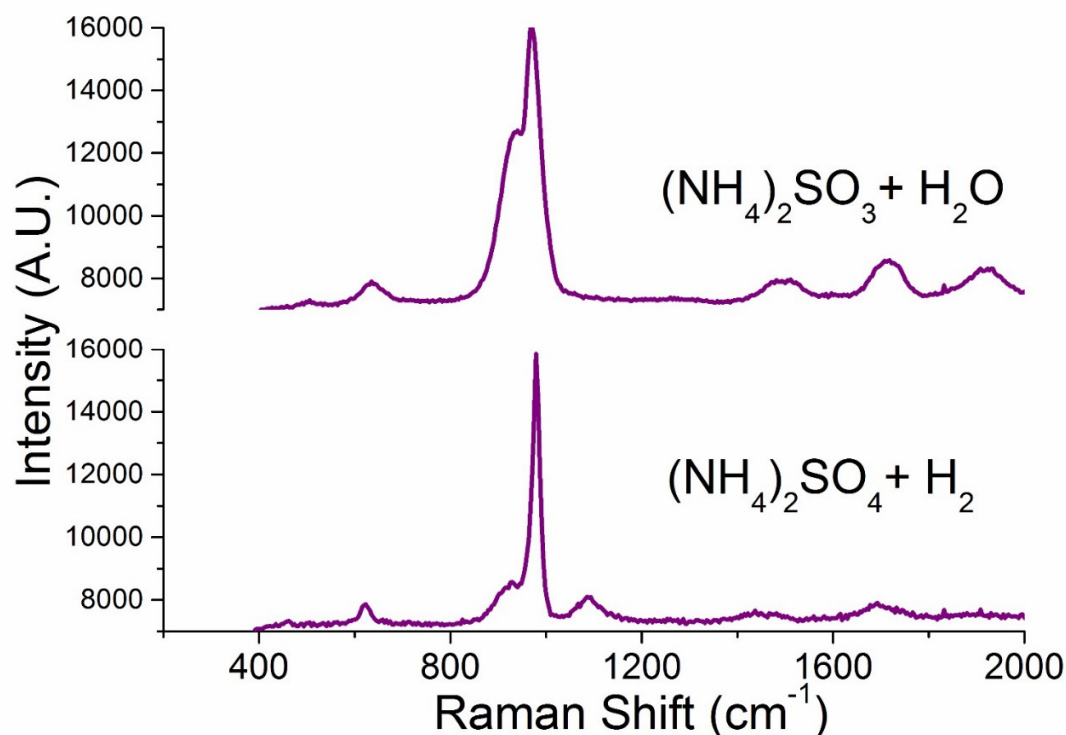


**Figure 1.** Raman spectra demonstrating the feasibility of photolytic oxidation in the solid state at  $25^\circ\text{C}$  using a 25 mW laser at 244 nm.

### 3.2 Vibrational Spectra of $(\text{NH}_4)_2\text{SO}_3 \cdot \text{H}_2\text{O}$

The Raman spectrum of  $(\text{NH}_4)_2\text{SO}_3 \cdot \text{H}_2\text{O}$  at 20 K is shown in **Figure 2** together with the Raman spectra of  $(\text{NH}_4)_2\text{SO}_4$  and  $\text{Na}_2\text{SO}_3$  for comparison. On closer examination of the lower part of **Figure 2**, it is noticeable that the modes were better resolved at low temperature,



since it is possible to observe the individual Raman bands assigned to the S-O stretching and O-S-O deformations modes. In the case of  $\nu_2$ , (*see* **Tables 1-3** for graphical representation of normal modes of vibrations) the Raman bands in  $(\text{NH}_4)_2\text{SO}_3 \cdot \text{H}_2\text{O}$  and  $(\text{NH}_4)_2\text{SO}_4$  are almost identical in intensity and were identified as two individual peaks *ca.* 448 and 460  $\text{cm}^{-1}$ . Note that despite contribution of sapphire to the first Raman band this could not solely be responsible of such peak, since its ratio of intensity does not correspond to the Raman spectrum of sapphire, as shown in the inset of **Figure 2**. A similar condition was found in the wagging mode of water at 647  $\text{cm}^{-1}$ , which is only present in the monohydrate, where intensity in absence of water is exclusively due to sapphire vibrations. Next to this, there is the  $\nu_4$  deformation band, exhibiting Raman peaks around 610 and 622  $\text{cm}^{-1}$ . Both the  $\nu_2$  and  $\nu_4$  bands were displaced to higher frequencies in  $\text{Na}_2\text{SO}_3$  *ca.* 498 and 638  $\text{cm}^{-1}$ , respectively. The most intense features in the Raman spectra correspond to the  $\nu_1$  mode characterised by 4 peaks at 973, 957, 923 and 909  $\text{cm}^{-1}$  in the monohydrate. Sodium sulfite exhibits a peak around 990  $\text{cm}^{-1}$  for this mode. Finally, the three peaks at 1043, 1083 and 1130  $\text{cm}^{-1}$  were assigned to the  $\nu_3$  vibrational mode [24, 25]. It is noteworthy that such bands were not visible at room temperature for the monohydrate.

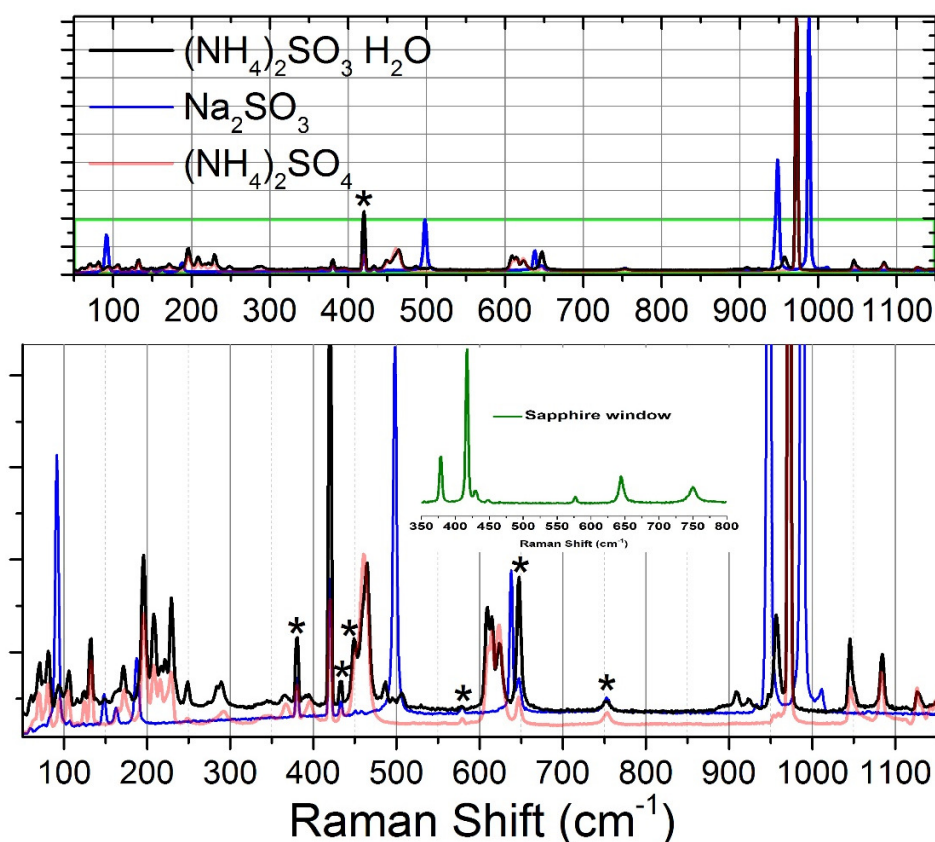


**Figure 2.** *Top:* Raman spectra of  $(\text{NH}_4)_2\text{SO}_3 \cdot \text{H}_2\text{O}$ ,  $(\text{NH}_4)_2\text{SO}_4$  and  $\text{Na}_2\text{SO}_3$  at 20K using 785 nm laser excitation. *Bottom:* Zoom into the lower spectral region. Note: Raman bands contributed by the optical window of the sample holder, made of sapphire, are denoted with a star; *i.e.* inset shows Raman spectrum of sapphire.

Whereas the Raman spectra are largely dominated by modes involving sulfur, INS intensities are determined by the amplitude of motion of the atoms in the mode and their incoherent scattering cross section. For  $^1\text{H}$ , both of these are large and modes involving hydrogen motion will dominate the spectrum. For non-hydrogenous materials, the strongest modes will generally involve the lightest atoms (since they will have the largest amplitude of motion). To provide a definitive assignment of the vibrational spectra, assignments from the literature were further supported by DFT calculations; the calculated vibrational modes are available in the supplementary material, so readers can easily visualize crystal vibrations using Jmol

[44]. In order to facilitate interpretation of the INS spectra, the theoretical and experimental results are overlaid. **Figure 3** shows the experimental INS spectrum obtained at TOSCA and two DFT-calculated spectra. The blue spectral contour was obtained by constraining the calculation to the lattice parameters reported in the literature for  $(\text{NH}_4)_2\text{SO}_3 \cdot \text{H}_2\text{O}$  and the green spectral contour was calculated by allowing both the lattice parameters and the geometry to freely optimise within CASTEP.

Better agreement was found when the experimental lattice parameters were used to calculate the spectrum. Although there are clear differences between the experimental and theoretical data, it is important to remind the reader that theoretical spectra were not corrected by any scale factor. At the very right of the experimental spectrum shown in **Figure 3**, is the bending mode of water at *ca.*  $1700 \text{ cm}^{-1}$ . The N-H deformation mode in ammonium ions occurs at  $1475 \text{ cm}^{-1}$ . Around  $900 \text{ cm}^{-1}$  there is an out of plane deformation of  $\text{O} \cdots \text{H} \cdots \text{O}$ . Then in order to simplify the interpretation five spectral sections are considered. The first covering from  $600$  to  $750 \text{ cm}^{-1}$  involves torsional vibrations of water; the following section in decreasing order goes from  $300$  to  $600 \text{ cm}^{-1}$  and it covers torsional vibrations of ammonium ions at  $323$ ,  $443$  and  $508 \text{ cm}^{-1}$ . Translational vibrations of ammonium ions and water are localised between  $175$  and  $300 \text{ cm}^{-1}$ . Torsional vibrations of sulfites/sulfates are generally seen in the spectral range,  $100 - 175 \text{ cm}^{-1}$ . Below the aforementioned, the crystal lattice vibrations are found [36,38].

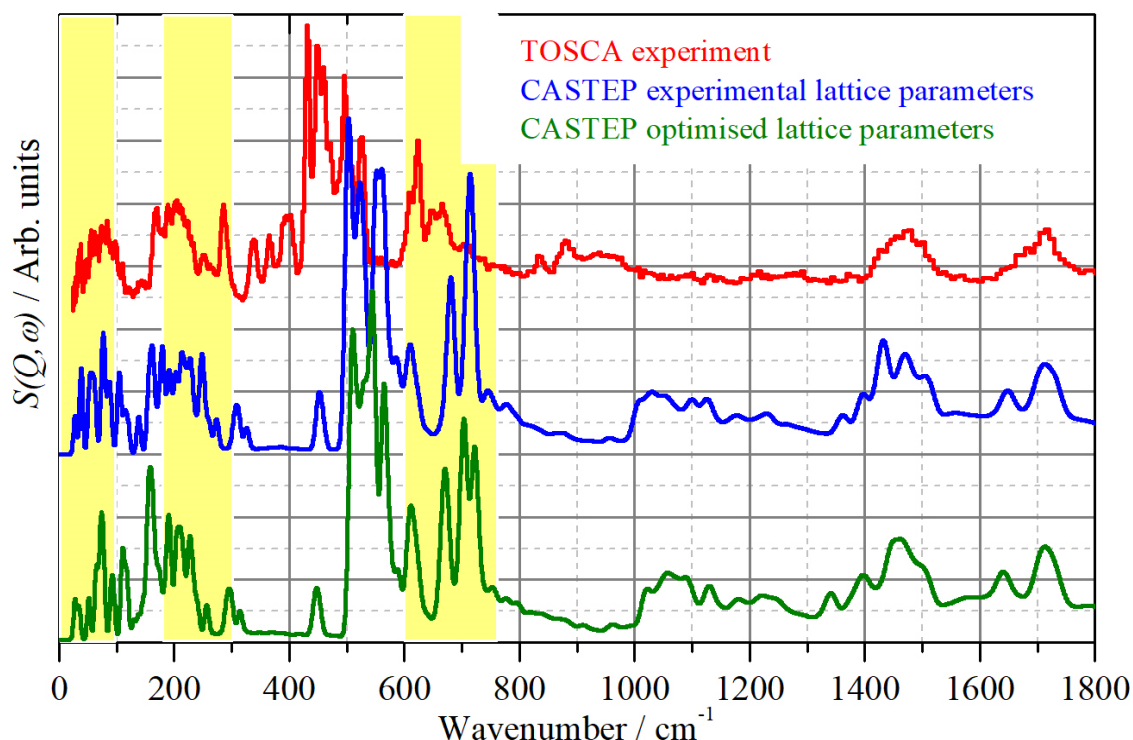


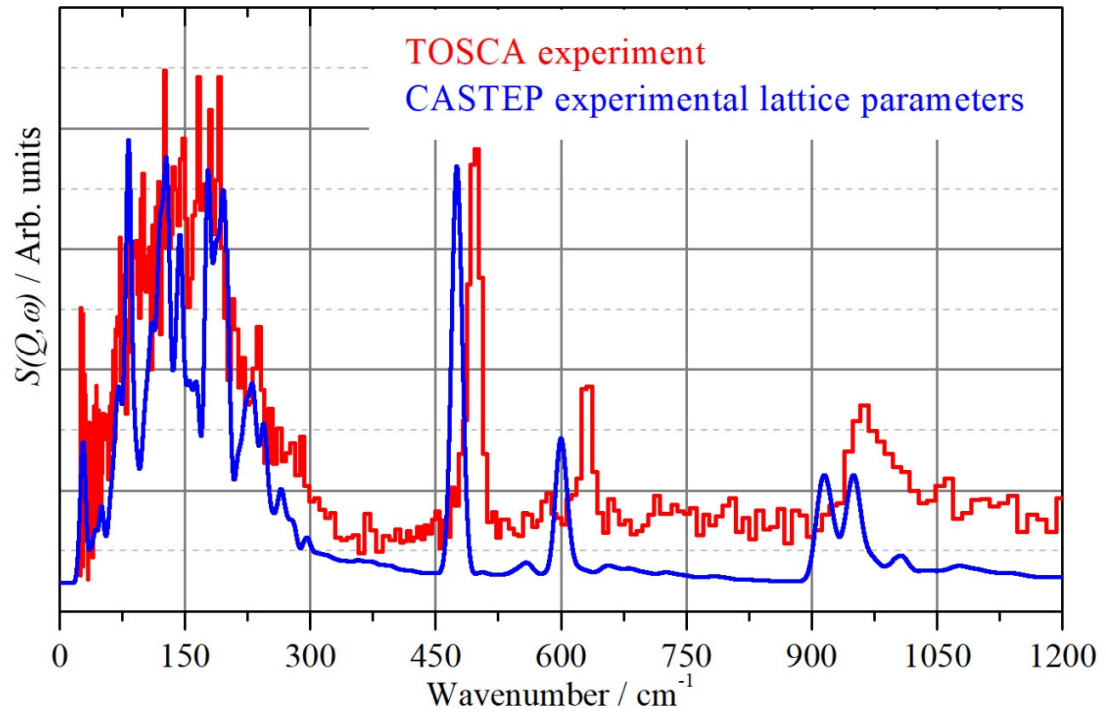
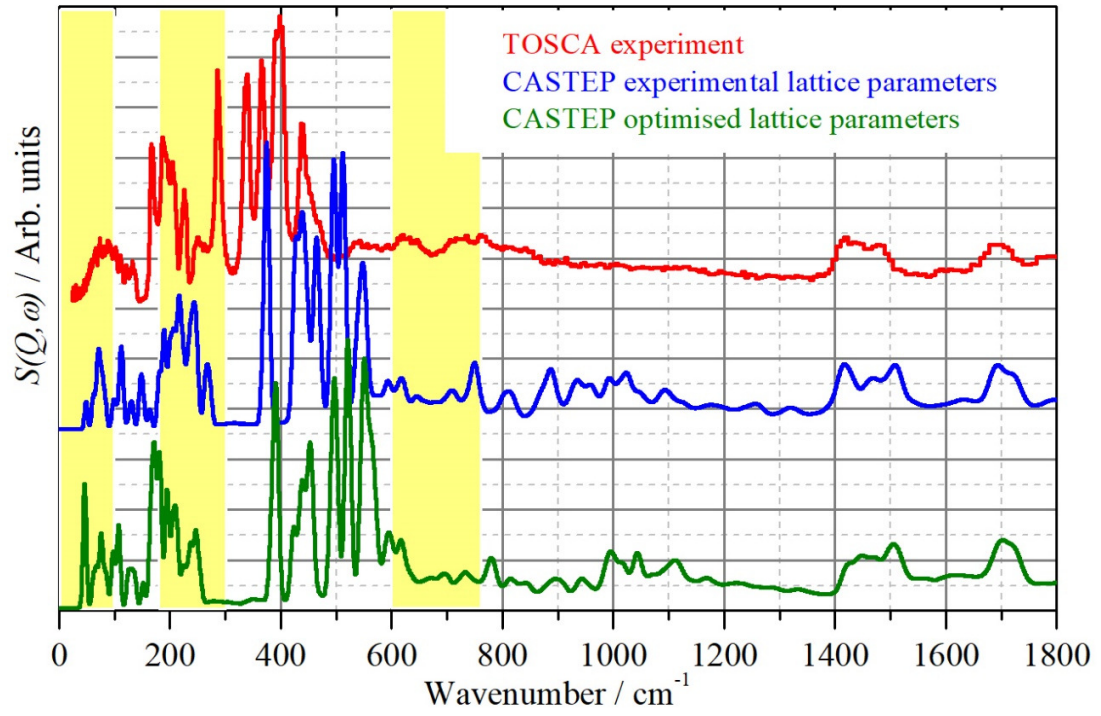
**Figure 3** INS spectra of  $(\text{NH}_4)_2\text{SO}_3 \cdot \text{H}_2\text{O}$ : Experimental taken at TOSCA at 20 K (red), Theoretical spectra (blue and green).

Based on these assignments,  $(\text{NH}_4)_2\text{SO}_4$  can also be interpreted. The INS spectra were similarly sectioned, as illustrated in the top part of **Figure 4**. Here, it was evident that the loss of features associated with water results in more relatively more intense peaks for the torsional vibration of sulfate and the translational vibrations of the ammonium ion, respectively. There is also a noticeably better correlation between experimental and theoretical data. However, the most remarkable correlation between experiment and theory is seen in the INS spectra of  $\text{Na}_2\text{SO}_3$ , shown in the bottom part of **Figure 4**, where, as predicted by the DFT calculations, it is possible to identify the bands conforming the S-O stretching and O-S-O deformations modes, previously observed for  $\text{Na}_2\text{SO}_3$  in **Figure 2**. Based on the calculated dispersion curves for  $\text{Na}_2\text{SO}_3$  (see supplementary information),

whereas the torsional vibrations of sulfite exhibited dispersion, the internal modes of vibration of sulfite, in absence of ammonium, were not dispersed.

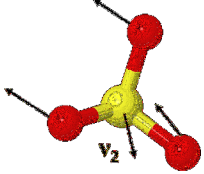
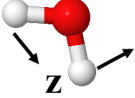
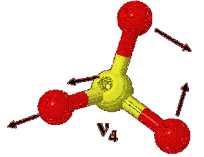
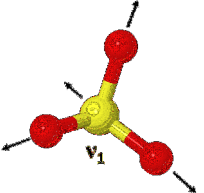
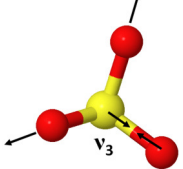
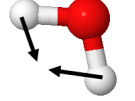
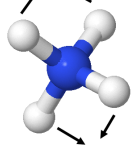
DFT provides a more accurate description of  $\text{Na}_2\text{SO}_3$  as compared to  $(\text{NH}_4)_2\text{SO}_3 \cdot \text{H}_2\text{O}$  and  $(\text{NH}_4)_2\text{SO}_4$  because there is no hydrogen bonding present. The failure of DFT to accurately reproduce the spectra of moderately strongly hydrogen bonded systems has been recognised previously for  $\text{H}_2\text{O}_2$  [47]. In this case the O–H bond was too long and the intermolecular hydrogen bond was too short, resulting in overbinding and the vibrational modes being shifted to higher energy, as also observed here for  $(\text{NH}_4)_2\text{SO}_3 \cdot \text{H}_2\text{O}$  and  $(\text{NH}_4)_2\text{SO}_4$ . A comparison of a variety of pseudopotentials and exchange-correlation functionals, showed that the error was largely in the latter. A similar cause is likely to be the case here.

**Tables 1-3** present the assignments for the salts investigated here.



**Figure 4** INS spectra of: *Top*:  $(\text{NH}_4)_2\text{SO}_4$ : Experimental taken at TOSCA at 20 K (red), Theoretical spectra (blue and green); and *Bottom*:  $\text{Na}_2\text{SO}_3$ : Experimental taken at TOSCA at 20 K (red), Theoretical spectra (blue).

**Table1.** Assignment of vibrational modes based on the Raman and INS spectra of  $(\text{NH}_4)_2\text{SO}_3 \cdot \text{H}_2\text{O}$ .

Frequency ( $\text{cm}^{-1}$ )	Assignment	Graphical Representation
448	$\nu_2 \text{ SO}_3$	
460	$\nu_2 \text{ SO}_3$	
647	Wagging $\text{H}_2\text{O}$	
610	$\nu_4 \text{ SO}_3$	
622	$\nu_4 \text{ SO}_3$	
900	Out of plane $\text{O} \cdots \text{H} \cdots \text{O}$ deformation	
973		
957		
923		
909		
1043	$\nu_3 \text{ SO}_3$	
1083	$\nu_3 \text{ SO}_3$	
1130	$\nu_3 \text{ SO}_3$	
1700	Bending $\text{H}_2\text{O}$	
1475	N-H deformation	
600 -750	Torsional vibrations $\text{H}_2\text{O}$	
300 – 600	Torsional vibrations $\text{NH}_4$	
175 - 300	Translational vibrations $\text{NH}_4 / \text{H}_2\text{O}$	
100 - 175	Torsional vibrations of $\text{SO}_3$	
<175	Crystal lattice vibrations	

**Table2.** Assignment of vibrational modes based on the Raman and INS spectra of  $(\text{NH}_4)_2\text{SO}_4$ .

Frequency ( $\text{cm}^{-1}$ )	Assignment	Graphical Representation
448	$\nu_2 \text{ SO}_4$	
460	$\nu_2 \text{ SO}_4$	
610	$\nu_4 \text{ SO}_4$	
622	$\nu_4 \text{ SO}_4$	
1475	N-H deformation	
300 – 600	Torsional vibrations $\text{NH}_4$	
175 - 300	Translational vibrations $\text{NH}_4$	
100 - 175	Torsional vibrations of $\text{SO}_4$	
<175	Crystal lattice vibrations	

**Table3.** Assignment of vibrational modes based on the Raman and INS spectra of  $\text{Na}_2\text{SO}_3$ .

Frequency ( $\text{cm}^{-1}$ )	Assignment	Graphical Representation
498	$\nu_2 \text{ SO}_3$	
638	$\nu_4 \text{ SO}_3$	
990	$\nu_1 \text{ SO}_3$	
< 250	Crystal lattice vibrations	



## 4. Conclusions

Photolytic oxidation of ammonium sulfite monohydrate in the solid state using a UV laser and observed with a Raman microscope was achieved at room temperature. However, we note that it is still necessary to demonstrate the feasibility under real conditions of solar irradiation.

Low-temperature Raman and INS spectra of  $(\text{NH}_4)_2\text{SO}_3 \cdot \text{H}_2\text{O}$ ,  $(\text{NH}_4)_2\text{SO}_4$  and  $\text{Na}_2\text{SO}_3$  were interpreted based on literature assignments or DFT calculations. The models here presented failed to correctly reproduce the hydrogen bonding due to the presence of ammonium and/or water. However, the INS spectra of  $\text{Na}_2\text{SO}_3$  exhibited very good agreement between experimental and theoretical data.

## 5. Acknowledgements

The authors acknowledge the financial support received from the Sector Fund CONACYT-SENER-ENERGY-SUSTAINABILITY 207450 within Strategic Project No. 10, entitled: “Solar Fuels & Industrial Processes”, by which it was possible to carry out experimental work in the UK and complete this manuscript to sustain this line of research. Also, our gratitude to Prof Felix Fernandez-Alonso, Dr Svemir Rudic and all the scientific, technical and administrative staff for the access and support provided during the operation of TOSCA at the ISIS Facility. The STFC Rutherford Appleton Laboratory is thanked for access to neutron beam facilities.

## 6. References

1. Duigou, A.L., et al., *HYTHEC: An EC funded search for a long term massive hydrogen production route using solar and nuclear technologies*. International Journal of Hydrogen Energy, 2007. **32**(10–11): p. 1516-1529.
2. M. Roeb, D. Thomey, D. Graf, C. Sattler, S. Poitou, F. Pra, et al. HycycleS: a project on nuclear and solar hydrogen production by sulphur-based thermochemical cycles. International Journal of Nuclear Hydrogen Production and Applications. 2011;2(3).
3. T-Raissi A, Muradov N, Huang C, Adebiyi O. Hydrogen from solar via light-assisted high-temperature water splitting cycles. Journal of Solar Energy Engineering. 2007;129(2):184-9
4. Huang C, Linkous CA, Adebiyi O, T-Raissi A. Hydrogen Production via Photolytic Oxidation of Aqueous Sodium Sulfite Solutions. Environmental Science & Technology. 2010;44(13):5283-8.
5. Deister U, Warneck P. Photooxidation of sulfite ( $\text{SO}_3^{2-}$ ) in aqueous solution. The Journal of Physical Chemistry. 1990;94(5):2191-8.
6. Yao W, Song X, Huang C, Xu Q, Wu Q. Enhancing solar hydrogen production via modified photochemical treatment of Pt/CdS photocatalyst. Catalysis Today. 2013;199:42-7.
7. Huang C. Solar hydrogen production via pulse electrolysis of aqueous ammonium sulfite solution. Solar Energy. 2013;91:394-401.
8. Taylor R, Davenport R, Talbot J, Herz R, Luc W, Genders D, et al. Status of the Solar Sulfur Ammonia Thermochemical Hydrogen Production System for Splitting Water. Energy Procedia. 2014;49:2047-58.
9. Vagia EC, Muradov N, Kalyva A, T-Raissi A, Qin N, Srinivasa AR, Kakosimos KE. Solar hybrid photo-thermochemical sulfur-ammonia water-splitting cycle: Photocatalytic hydrogen production stage. International Journal of Hydrogen Energy. 2017;42:20608-24
10. Kalyva AE, Vagia ECh, Konstandopoulos AG, Srinivasa AR, T-Raissi A, Muradov N, Kakosimos KE. Particle model investigation for the thermochemical steps of the sulfur-ammonia water splitting cycle. International Journal of Hydrogen Energy. 2017;42:3621-9
11. Long X-l, Li W, Xiao W-d, Yuan W-k. Novel homogeneous catalyst system for the oxidation of concentrated ammonium sulfite. Journal of Hazardous Materials. 2006;129(1–3):260-5.
12. Gao X, Du Z, Ding H-l, Wu Z-l, Lu H, Luo Z-y, et al. Effect of gas–liquid phase compositions on  $\text{NO}_2$  and  $\text{NO}$  absorption into ammonium-sulfite and bisulfite solutions. Fuel Processing Technology. 2011;92(8):1506-12.
13. Wu X, Kong F, Huang M, Yu S. Effects of pH on the formation of 4(5)-Methylimidazole in glucose/ammonium sulfate and glucose/ammonium sulfite caramel model reactions. Food Research International. 2015;76, Part 3:661-5.
14. Mazzei L, Cianci M, Benini S, Bertini L, Musiani F, Ciurli S. Kinetic and structural studies reveal a unique binding mode of sulfite to the nickel center in urease. Journal of Inorganic Biochemistry. 2016;154:42-9.

15. Lidong W, Juan W, Peiyao X, Qiangwei L, Wendi Z, Shuai C. Selectivity of transition metal catalysts in promoting the oxidation of solid sulfites in flue gas desulfurization. *Applied Catalysis A: General*. 2015;508:52-60.
16. Jao P, Xu F, Li J, Duan N, Chen G, Jiang L. The inhibition effect of  $\text{SeO}_2$  on hydrogen evolution reaction in  $\text{MnSO}_4\text{-(NH}_4)_2\text{SO}_4$  solution. *International Journal of Hydrogen Energy*. 2016;41:784-91
17. Jao P, Duan N, Zhang C, Xu F, Chen G, Li J, Jiang L. The effect of cobalt ion on the hydrogen evolution reaction in sulfate solution. *International Journal of Hydrogen Energy*. 2016;41:17793-800
18. Tara J. Fortin, John E. Shilling, Tolbert MA. Infrared spectroscopic study of the low-temperature phase behavior of ammonium sulfate. *Journal of geophysical research*. 2002;107:AAC 4-1–AAC 4-9.
19. Kanno H, Hiraishi J. Correlation of the Raman  $\nu_1$  bands of aquated divalent metal ions with the cation–hydrated water distance. *journal of Raman spectroscopy*. 1987;18:157-61.
20. Rudolph WW. Raman and Infrared Spectroscopic Investigation of Speciation in  $\text{BeSO}_4\text{(aq)}$ . *Journal of Solution Chemistry*. 2010;39(7):1039-59.
21. Rudolph W, Irmer G. Raman and infrared-spectroscopic investigations of dilute aqueous phosphoric acid solutions. *Journal of Solution Chemistry*. 1994;23(6).
22. Degen IA, Newman GA. Raman spectra of inorganic ions. *Spectrochemical Acta* 1992;49A:659-887.
23. Rudolph WW, Irmer G. Raman Spectroscopic Investigation of Speciation in  $\text{MnSO}_4\text{(aq)}$ . *Journal of Solution Chemistry*. 2014;43(3):465-85.
24. Mabrouk K., Kauffmann T., Aroui H., M. F. Raman study of cation effect on sulfate vibration modes in solid state and in aqueous solutions. *J Raman Spectrosc*. 2013(44):1603–8.
25. Rintoul L, Crawford K, Shurvell HF, Fredericks PM. Surface-enhanced Raman scattering of inorganic oxoanions. *Vibrational Spectroscopy*. 1997;15(2):171-7.
26. Ramos-Sanchez VH, Jeans R J, Devonshire R. Raman scattering studies of the condensed phase of the  $\text{HI}_x$  feed of the sulfur–iodine thermochemical cycle. *International Journal of Energy Research*. 2011;35:189–208
27. Spadoni A, Falconieri M, Lanchi M, Liberatore R, Marrocco M, Sau GS, Tarquini P. Iodine compounds speciation in  $\text{HI}$ – $\text{I}_2$  aqueous solutions by Raman spectroscopy. *International Journal of Hydrogen Energy*. 2012;37(2):1326-1334
28. Tyagi D, Varma S, Bhattacharya K, Jain D, Tripathi AK, Pillai CGS, Bharadwaj SR. Iodine speciation studies on Bunsen reaction of  $\text{S}$ – $\text{I}$  cycle using spectroscopic techniques. *International Journal of Hydrogen Energy*. 2012;37(4):3621-3625
29. Ting VP, Ramirez-Cuesta AJ, Bimbo N, Sharpe JE, Noguera-Diaz A, Presser V, Rudic S, Mays TJ. Direct evidence for solid-like hydrogen in a nanoporous carbon hydrogen storage material at supercritical Temperatures. *ACSNano*. 2015;9(8):8249-8254
30. Giddey S, Badwal SPS, Kulkarni A. Review of electrochemical ammonia production technologies and materials. *International Journal of Hydrogen Energy*. 2013;38(34):14576-94.
31. Smirnov LS, Natkaniec I, Johnson MR, Ivanov AS, Troyanov SI. Vibrational modes of hydrogen in  $(\text{NH}_4)_2\text{H}_5(\text{PO}_4)_2$  (Neutron scattering and simulation). *Crystallography Reports*. 2009;54(3):477-82.

32. Adams MA, Refson K, Gabrys BJ. The high resolution inelastic neutron scattering spectrum of ammonium fluoride. *Physical Chemistry Chemical Physics*. 2005;7(21):3685-92.
33. Rubín J, Palacios E, Bartolomé J, Tomkinson J, Fourquet JL.  $\text{NH}_4^+$  translational and librational spectrum in  $\text{NH}_4\text{AlF}_4$ . *Physica B: Condensed Matter*. 1992;180:723-5.
34. Novak DM, Smirnov LS, Kolesnikov AI, Voronin VI, Berger IF, Laptash NM, et al. Refinement of the crystal structure of the high-temperature phase G 0 in  $(\text{NH}_4)_2\text{WO}_2\text{F}_4$  (powder, X-ray, and neutron scattering). *Crystallography Reports*. 2013;58(1):129-34.
35. Tomkinson J, Kearley GJ. Phonon wings in inelastic neutron scattering spectroscopy: The harmonic approximation. *Journal of Chemical Physics*. 1989(91):5164.
36. Lipiński I., Kuriata J., Natkaniec I., A. P. Neutron Scattering Study of Sodium Ammonium Sulphate Dihydrate. *Phys Stat Sol*. 2001;227(2):477–83.
37. Jacobs WPJH, van Santen RA, Jobic H. Inelastic neutron scattering study of  $\text{NH}_4\text{Y}$  zeolites. *Journal of the Chemical Society, Faraday Transactions*. 1994;90(8):1191-6.
38. Tomkinson J, Kearley GJ. The effect of recoil of chemically distinct molecular ions on inelastic neutron scattering spectra of molecular vibrations. *Physica B: Condensed Matter*. 1992;180:665-7.
39. Adams M, A., Parker S. F., Fernandez-Alonso F., Cutler D. J. Cutler, Hodges C., King A., Simultaneous Neutron Scattering and Raman Scattering. *Applied Spectroscopy* 2009;63(7):727 - 32.
40. Clark S. J., Segall M. D., Pickard C. J., Hasnip P. J., Probert M. J., Refson K., Payne M. C. First principles methods using CASTEP, *Zeitschrift fuer Kristallographie* 220(5-6) pp. 567-570 (2005)
41. Battelle. *Acta Crystallographic*. 1965;19(4):491-692.
42. Villars P, Cenzual K, Daams J, Gladyshevskii R, Shcherban O, Dubenskyy V, et al.  $\text{Na}_2\text{SO}_3$ . In: Villars P, Cenzual K, editors. *Structure Types Part 9: Space Groups* (148) R-3 - (141) I41/amd. Berlin, Heidelberg: Springer Berlin Heidelberg; 2010. p. 209.
43. Udalova VVAp. *Kristallografiya*. Soviet Phys Cryst. 1964;8(538).
44. K. Refson, S. J. Clark and P. R. Tulip, Variational density functional perturbation theory for dielectrics and lattice dynamics. *Phys. Rev. B* 2006, 73(15), 155114.
45. Jmol: an open-source Java viewer for chemical structures in 3D.  
<http://www.jmol.org/>
46. Ramirez-Cuesta AJ. aCLIMAX 4.0.1, The new version of the software for analyzing and interpreting INS spectra. *Computer Physics Communications*. 2004;157(3):226-38.
47. P.W. Albers, J. Glenneberg, K. Refson and S.F. Parker, IINS study of the molecular properties of pure hydrogen peroxide and its water mixtures of different concentration, *Journal of Chemical Physics* 140 (2014) 16450.